Construction of photoresponsive RNA for photoswitching RNA hybridization†

Hiroshi Ito,[a] Xingguo Liang,*[a] Hidenori Nishioka[a] and Hiroyuki Asanuma*[a,b]

Received 15th July 2010, Accepted 9th September 2010
DOI: 10.1039/c0ob00432d

By introducing azobenzenes into RNA using D-threoninol as a scaffold, a photoresponsive RNA was constructed for efficiently photoswitching the formation and dissociation of RNA/RNA duplexes. The difference in melting temperature (T_m) between the *trans* and *cis* forms was so large that efficient photoregulation of RNA hybridization became possible, irrespective of the sequence adjacent to the introduced azobenzene. Compared to the corresponding photoresponsive DNA, the photoregulatory efficiency of azobenzene-modified RNA was even higher due to the drastic destabilization by *cis*-azobenzene. Structural analysis by NMR and molecular modeling indicated that the planar *trans*-azobenzene could not stabilize the RNA/RNA duplex with a rigid A-form structure by base pair stacking. However, the large steric hindrance caused by nonplanar *cis*-azobenzene was quite effective at distorting and destabilizing the duplex structure. We also discuss the effect of methylation of azobenzene at the *ortho* positions on photoregulation of RNA/RNA duplex formation. This newly constructed photoresponsive RNA has promising applications such as photoswitching of RNA functions.

Introduction

Recently, the biological roles of small RNA molecules[1] have attracted much attention due to continued discoveries of various functional RNAs such as ribozymes,[2] microRNA (miRNA),[3] and short interfering RNA (siRNA).[4] These functional RNAs, also called non-coding RNAs, are well conserved in many species and are involved in many important bioreactions, especially for the regulation of gene expression. It is believed that gene silencing with functional RNAs will be applied therapeutically in the near future with even higher efficiency than antisense strategies using chemically synthesized oligonucleotides.[5] Accordingly, the artificial control of RNA functions with external stimuli, such as light, should become important for spaciotemporal control of gene expression as well as the enhancement of efficiency and specificity.[6] More interestingly, these functional RNAs have to take a particular conformation to exert their potential. For example, the hammerhead structure of the hammerhead ribozyme is essential for cleaving target mRNAs,[2] and the RNA/RNA duplex of siRNAs that forms the active ribonucleoprotein complex RISC (RNA induced silencing complex) is the key component in the RNA interference (RNAi) pathway.[4b] If the formation of these functional RNA structures can be artificially regulated, their functions can be easily controlled.

In our previous work, we synthesized azobenzene-tethered DNA with D-threoninol as a scaffold and demonstrated reversible photoregulation of the formation and dissociation of DNA duplexes.[7] The mechanism of photoregulation can be described as follows: the planar *trans*-azobenzene intercalates between the two adjacent base pairs and stabilizes the DNA duplex by stacking interactions, whereas the nonplanar *cis*-azobenzene destabilizes the duplex by steric hindrance. Based on this photoregulation strategy, the photoswitching of various DNA functions such as DNA primer extension,[7b] hybridization for driving DNA nanomachines,[8] and other enzymatic reactions[7b] has been achieved. Furthermore, we found that the modification of azobenzene with methyl groups at its *ortho* positions significantly improved photoregulatory efficiency:[9] *trans*-2′,6′-dimethylazobenzene increased stabilization of the duplex, whereas the *cis*-form destabilized it more than did unmodified azobenzene.

In the present study, in order to develop a method for controlling various RNA functions, we constructed photoresponsive RNAs by tethering azobenzene *via* D-threoninol. RNA hybridization was successfully photoregulated by the photoisomerization of the introduced azobenzene. We also clarified the mechanism for photoregulation of RNA hybridization by thermodynamic and structural analysis. Finally, the effect of methylation of azobenzene on the photoresponsiveness was also investigated.

Results and discussion

Photoregulation of RNA/RNA duplex formation by introducing azobenzene to RNA

Photoresponsive RNA was synthesized by introducing azobenzene *via* D-threoninol using standard phosphoramidite chemistry as reported previously.[7a] The sequences of azobenzene-modified RNA are shown in Scheme 1. First, the photoisomerization of introduced azobenzene was investigated by UV–Vis spectroscopy. As shown in Fig. 1a, *trans-cis* isomerization of azobenzene was confirmed by using UV–Vis spectroscopy (Fig. 1a). Upon irradiation with visible light ($\lambda > 400$ nm), the introduced azobenzene had a strong absorption around 340 nm (π–π^* transition) indicating that most of the azobenzenes (more than 90%) were in the *trans* form (solid line in Fig. 1a). After irradiation with UV light (320–380 nm), the absorbance at 340 nm remarkably decreased (dotted

[a]*Graduate School of Engineering, Nagoya University, Furo-cho, Chikusa, Nagoya, 464-8603, Japan. E-mail: liang@mol.nagoya-u.ac.jp, asanuma@mol.nagoya-u.ac.jp; Fax: (+81)52-789-2528; Tel: (+81)52-789-2488*
[b]*Core Research for Evolution Science and Technology (CREST), Japan Science and Technology (JST), Kawaguchi, Saitama, 332-0012, Japan*
† Electronic supplementary information (ESI) available: UV–Vis, CD and NMR spectra of azobenzene-modified DNA duplex; detailed spectral data for **R_XG/R_cC**; molecular modelling of **NMR-R_X/NMR-R_c**. See DOI: 10.1039/c0ob00432d

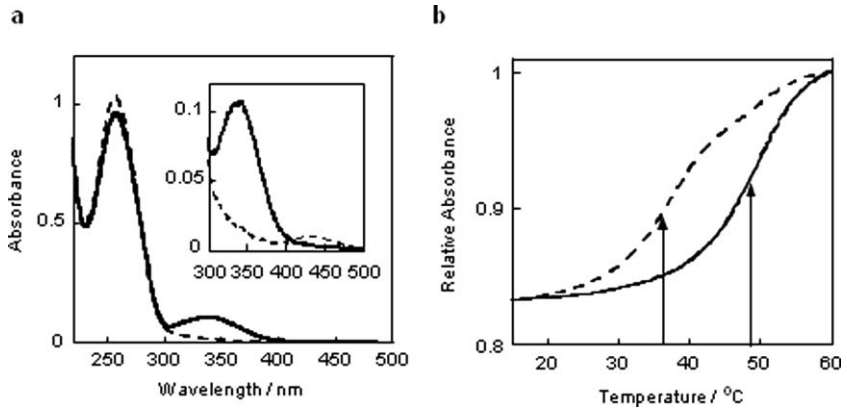

Fig. 1 UV–Vis spectra (a) and melting curves (b) of $\mathbf{R_XG/R_cC}$ with *trans*-azobenzene (solid line) and *cis*-azobenzene (dotted line). Conditions: 5 μM dsRNA, 100 mM NaCl, 10 mM phosphate buffer (pH 7.0). The introduced azobenzene was isomerized to *trans*-form with visible light ($\lambda > 440$ nm), and to *cis*-form with UV light (320–380 nm), respectively.

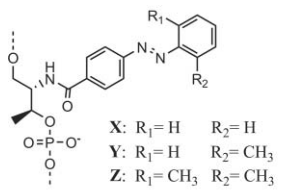

$\mathbf{D_XG}$ 5'-CTTAC**X**GCTGA-3'
$\mathbf{D_YG}$ 5'-CTTAC**Y**GCTGA-3'
$\mathbf{D_ZG}$ 5'-CTTAC**Z**GCTGA-3'

$\mathbf{D_nG}$ 5'-CTTAC GCTGA-3'
$\mathbf{D_cC}$ 3'-GAATG CGACT-5'

$\mathbf{R_XG}$ 5'-CUUAC**X**GCUGA-3'
$\mathbf{R_cC}$ 3'-GAAUG CGACU-5'
$\mathbf{R_XA}$ 5'-CUUAC**X**ACUGA-3'
$\mathbf{R_cU}$ 3'-GAAUG UGACU-5'
$\mathbf{R_XU}$ 5'-CUUAC**X**UCUGA-3'
$\mathbf{R_cA}$ 3'-GAAUG AGACU-5'
$\mathbf{R_XC}$ 5'-CUUAC**X**CCUGA-3'
$\mathbf{R_cG}$ 3'-GAAUG GGACU-5'

$\mathbf{R_nG}$ 5'-CUUAC GCUGA-3'
$\mathbf{2R_X}$ 5'-CUU**X**ACGC**X**UGA-3'

NMR-R$_X$ 5'-CGA**X**GUC-3'
NMR-R$_c$ 3'-GCU CAG-5'

$\mathbf{R_YG}$ 5'-CUUAC**Y**GCUGA-3'
$\mathbf{R_ZG}$ 5'-CUUAC**Z**GCUGA-3'

Scheme 1 Sequences of DNA and RNA used in this study. The structure of the azobenzene residue is also shown.

line in Fig. 1a) indicating that *trans*-azobenzene was promptly isomerized to the *cis*-form (about 80%). The photoisomerization was completely reversible, and no decomposition was observed during repetitive light irradiation (data not shown).

To evaluate the photoregulatory efficiency of RNA hybridization using azobenzene-tethered RNA, we investigated the thermal stability change of RNA/RNA duplexes induced by the *trans*–*cis* isomerization of the introduced azobenzene. For duplex $\mathbf{R_XG/R_cC}$, the T_m for the *trans*-form was 48.8 °C as determined from its melting curve (solid line in Fig. 1b). After the azobenzene was isomerized to the *cis*-form, the T_m decreased to 36.5 °C (dotted line in Fig. 1b), demonstrating that *cis*-azobenzene significantly destabilized the RNA/RNA duplex. The T_m change (ΔT_m) by *trans*–*cis* photoisomerization, being used as an indicator to evaluate photoregulatory efficiency, was as large as 12.3 °C and the difference in the change of free energy between the *cis*- and *trans*-forms (Δ (Δ*G*)) was 9.8 KJ/mol (Supplemental Table S1†). This value was much larger than that of the corresponding DNA/DNA duplex ($\mathbf{D_XG/D_cC}$) whose ΔT_m was 7.3 °C (Table 1; see Supplemental Fig. S2† for the T_m curves). These results indicated that RNA/RNA hybridization can be efficiently photoregulated by using azobenzene-tethered RNA.

Compared to the native RNA/RNA duplex $\mathbf{R_nG/R_cC}$ (T_m = 50.7 °C), the azobenzene-modified duplex, *trans*-$\mathbf{R_XG/R_cC}$, showed a slightly lower T_m, indicating that even *trans*-azobenzene destabilized the duplex to some extent (Table 1). In the case

Table 1 Melting temperatures (T_ms) of RNA/RNA, DNA/DNA, RNA/DNA, and DNA/RNA duplexes

Duplex	T_m/°C[a]		
	trans	*cis*	ΔT_m[b]
$\mathbf{R_XG/R_cC}$	48.8	36.5	12.3
$\mathbf{D_XG/D_cC}$	42.9	35.6	7.3
$\mathbf{2R_X/R_cC}$	44.9	21.0	23.9
$\mathbf{R_XG/D_cC}$	34.3	25.0	9.3
$\mathbf{D_XG/R_cC}$	41.1	30.0	11.1
$\mathbf{R_nG/R_cC}$	50.7[c]		
$\mathbf{D_nG/D_cC}$	40.9[c]		
$\mathbf{R_nG/D_cC}$	34.2[c]		
$\mathbf{D_nG/R_cC}$	40.9[c]		

[a] Conditions: 5 μM dsDNA or dsRNA, 100 mM NaCl, 10 mM phosphate buffer (pH 7.0). [b] Change of T_m induced by *cis*–*trans* photoisomerization. [c] T_m values of native duplexes with only natural nucleotides. The sequences are shown in Scheme 1. The value of the measurement error was estimated within ± 0.3 °C.

of DNA/DNA duplexes however, the T_m of *trans*-$\mathbf{D_XG/D_cC}$ (42.9 °C) was 2.0 °C higher than that of $\mathbf{D_nG/D_cC}$ (40.9 °C), demonstrating that the attached *trans*-azobenzene stabilized the DNA duplex. As described previously, this stabilization effect was attributed to the stacking effect of the planar and hydrophobic *trans*-azobenzene with adjacent DNA base pairs.[7b,10] The destabilization effect of *trans*-azobenzene in the case of RNA/RNA duplexes indicates that it does not stack well with base pairs. This can be explained by the fact that the rigid A-form structure of the RNA/RNA duplex does not easily accept intercalators between the base pairs.[11] However, a red shift upon duplex formation was observed in the region of 300–400 nm (Supplemental Fig. S3†), indicating that the azobenzene moiety did not flip out completely from the duplex.

On the other hand, the nonplanar *cis*-azobenzene drastically destabilized the RNA/RNA duplex. As shown in Table 1, the T_m of *cis*-$\mathbf{R_XG/R_cC}$ was lower than that of the corresponding native RNA/RNA duplex by 14.2 °C. However, the difference in T_m between *cis*-$\mathbf{D_XG/D_cC}$ and the native DNA duplex was only 5.3 °C. Compared to DNA duplexes, the *cis*-azobenzene might cause larger steric hindrance for RNA/RNA duplexes and more free energy lost during duplex formation by tethering nonplanar

cis-azobenzene to the rigid A-form structure. This effect was enhanced in the case of **2R$_X$/R$_c$C**, in which two azobenzenes were introduced (See Scheme 1 for the sequence). As shown in Table 1, the T_m of *cis*-**2R$_X$/R$_c$C** was 29.7 °C lower than that of the native RNA/RNA duplex. Consequently, the large destabilization effect of *cis*-azobenzene should be the main mechanism for obtaining efficient photoregulation of RNA hybridization. For **2R$_X$/R$_c$C**, the ΔT_m between the *trans*- and *cis*-forms was as large as 23.9 °C. Accordingly, clear-cut photoregulation of RNA hybridization is attainable by introducing multiple azobenzenes.

Efficient photoregulation was also attained for an RNA/DNA duplex, which usually has an A-form structure, when azobenzene was introduced into either the RNA or DNA strand (Table 1). For both cases (**R$_X$G/D$_c$C** and **D$_X$G/R$_c$C**), a larger ΔT_m was obtained than for the DNA/DNA duplex, indicating again that introducing azobenzene into an A-form duplex is favourable for photoregulation. Interestingly, no destabilization effect of *trans*-azobenzene was observed in either case. Thus, introducing azobenzene into an oligonucleotide (either RNA or DNA) *via* D-threoninol can be used as a common, facile, and robust tool for photoregulating the functions of nucleic acids.

Dependency of photoregulatory efficiency on the sequence adjacent to the introduced azobenzene

We also investigated the sequence dependency of photoregulation of RNA hybridization. Assuming that the stability of an RNA/RNA duplex involving azobenzene depends mainly on the base pairs adjacent to azobenzene,[12] we investigated four sequences in which the base at the 3′-side was systematically changed. The photoregulatory efficiency was also evaluated by the ΔT_m between the *trans* and *cis* forms. As shown in Table 2, for all RNA/RNA duplexes, the ΔT_m was above 9.0 °C, demonstrating that a photoresponsive RNA involving azobenzene can generally be used for efficiently photoregulating RNA hybridization. On the other hand, the ΔT_m changes to some extent with the sequence. For example, **R$_X$C/R$_c$G** showed a smaller ΔT_m (9.1 °C) than **R$_X$G/R$_c$C** by 3.2 °C, although they had the same GC content. The ΔT_m tended to be larger when a purine nucleobase, G or A, was adjacent to the azobenzene (**R$_X$G/R$_c$C**, **R$_X$A/R$_c$U**). The larger size of purines at the azobenzene-modified strand may contribute to the larger steric hindrance caused by *cis*-azobenzene.

Table 2 Sequence dependency of photoregulatory efficiency

Duplex[a]	T_m/°C[b] *trans*	T_m/°C[b] *cis*	ΔT_m
R$_x$G/R$_c$C	48.8	36.5	12.3
R$_x$A/R$_c$U	41.8	29.4	12.4
R$_x$U/R$_c$A	41.6	31.2	10.4
R$_x$C/R$_c$G	46.1	37.0	9.1

[a] The sequences are shown in Scheme 1. [b] Conditions: 5 μM dsRNA, 100 mM NaCl, 10 mM phosphate buffer (pH 7.0). The value of the measurement error was estimated within ± 0.3 °C.

Structural analysis of RNA/RNA duplexes involving azobenzene

In order to obtain structural information on azobenzene-modified RNA/RNA duplexes, circular dichroism (CD) spectroscopy, ^{1}H-NMR analysis, and molecular modelling were carried out. First, CD spectra of **R$_X$G/R$_c$C** were measured to uncover the induced CD of the azobenzene moiety. As shown in Fig. 2, a typical CD of an A-form duplex structure was observed at the region of absorption of nucleobases (200–260 nm), demonstrating that the introduction of azobenzene did not cause a big change in the RNA/RNA duplex structure. At the region of azobenzene absorption (300–500 nm), a very weak induced CD (positive for π–π* transition and negative for n-π* transition) appeared after the duplex formed at 0 °C for both the *trans*- and *cis*-forms. This result shows that the corresponding π–π* transition moment on the plane of *trans*-azobenzene was parallel to the plane of the base pairs.[13] Interestingly, in the case of DNA/DNA duplexes involving one azobenzene, the induced CD at 300–500 nm was reversed: slightly negative for the π–π* transition and positive for the n-π* transition (Supplemental Fig. S4†).

To obtain more information about the position of azobenzene in the RNA/RNA duplexes, 1D and 2D ^{1}H-NMR spectra of a 6-bp long duplex, **NMR-R$_X$/NMR-R$_c$**, were measured in which the introduced azobenzene was *trans*-form (see Scheme 1 for the sequence). The above sequence was used because the NMR structure of an azobenzene-modified DNA duplex with the same

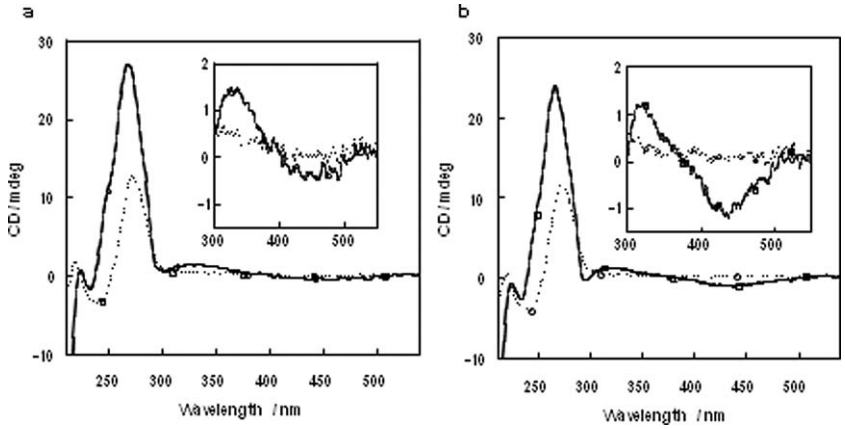

Fig. 2 CD spectra of the *trans*-**R$_X$G/R$_c$C** duplex (a) and *cis*-**R$_X$G/R$_c$C** (b) at 0 °C (solid lines) and 60 °C (dotted lines). Conditions: 5 μM dsRNA, 100 mM NaCl, 10 mM phosphate buffer (pH 7.0).

sequence was determined previously.[10] From the NMR signals of NOESY, DQF-COSY, and TOCSY, most of the protons in the duplex were assigned. As shown in Fig. 3a, the assignment of imino protons (11–14 ppm) could be verified from the 1D and NOESY spectra measured in H_2O (H_2O/D_2O = 9/1). Only four strong signals of imino protons were observed because the two imino protons (G^7 and G^{12}) at both ends are usually very weak and broad due to rapid exchange with water. From the NOEs between imino protons, the four individual signals were assigned as shown in Fig. 3a. The fact that all four peaks are sharp indicates that the introduced azobenzene moiety did not interfere with the base pairing in the RNA/RNA duplex. Furthermore, an NOE between U^{10} and G^4 was not observed, probably because the intercalated azobenzene separates the two base pairs.

Compared to U^5, the signal of the imino proton in U^{10} shifted greatly to a higher magnetic field, indicating that one benzene ring of azobenzene was located above or below the imino proton of U^{10}. NOEs signals between the imino proton of U^{10} and aromatic protons on azobenzene were also observed, although they were not so strong. On the other hand, the signal of G^4 did not shift to a higher magnetic field compared to that of G^2, although strong NOE signals between the imino proton of G^4 and the H2 (H6) and H8 (H12) protons on azobenzene were observed. This indicated that the N=N double bond of azobenzene is located close to the imino proton of G^4. All of the above results demonstrate that *trans*-azobenzene is located between two adjacent base pairs but is not flipped out completely from the duplex. However, the duplex was not stabilized compared to the native RNA/RNA duplex, probably because the azobenzene only partially stacked with the adjacent base pairs. In the case of the azobenzene-modified DNA duplex, both T^{10} and G^4 showed much larger upfield shifts because azobenzene could stack well with both the adjacent base pairs, and the DNA duplex was obviously stabilized (Supplemental Fig. S5†).

Finally, we performed molecular modelling to obtain an energy-minimized structure of RNA/RNA duplexes involving azobenzene (Fig. 4). Compared to the native RNA/RNA duplex, the *trans*-azobenzene distorted the duplex to some extent, although it partially intercalated between adjacent base pairs. The slight destabilization effect of *trans*-azobenzene can be explained by insufficient stacking interactions between the hydrophobic azobenzene and the base pairs. From another viewpoint, complete intercalation cannot be obtained because it might cause too much stress in the backbone due to the insertion of the azobenzene residue *via* D-threoninol. In the case of nonplanar *cis*-azobenzene,

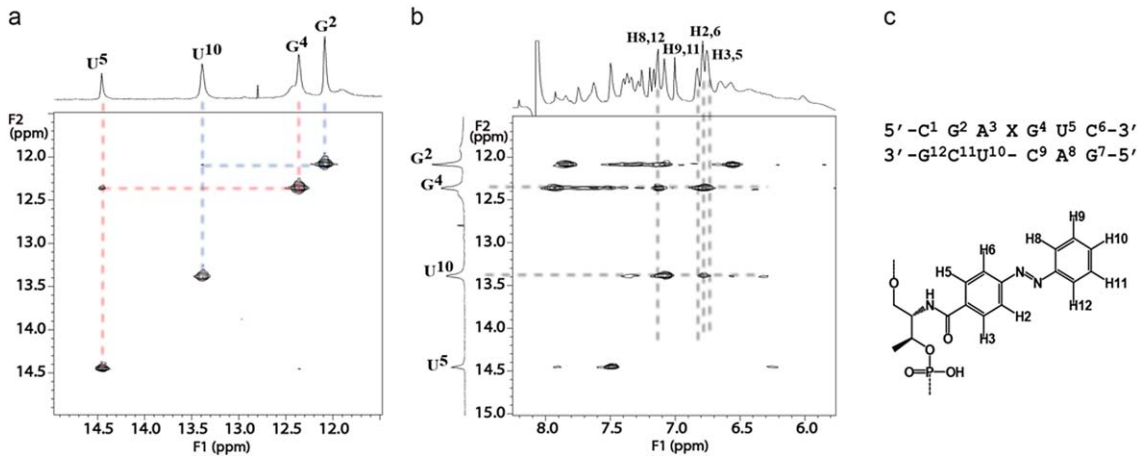

Fig. 3 2D NOESY spectra of duplex **NMR-R_X/NMR-R_c** at the imino proton region (a) and at the region between signals of aromatic protons (6.0–8.0 ppm) and those of imino protons (12–15 ppm) (b). Conditions: 1.0 mM dsRNA, H_2O/D_2O 9/1 at 278 K (mixing time = 150 ms), 200 mM NaCl, 20 mM phosphate buffer (pH 7.0). Assignments of each proton are denoted on the projected 1D spectrum. The residue numbers for imino protons and proton numbers for azobenzene are designated as shown in (c).

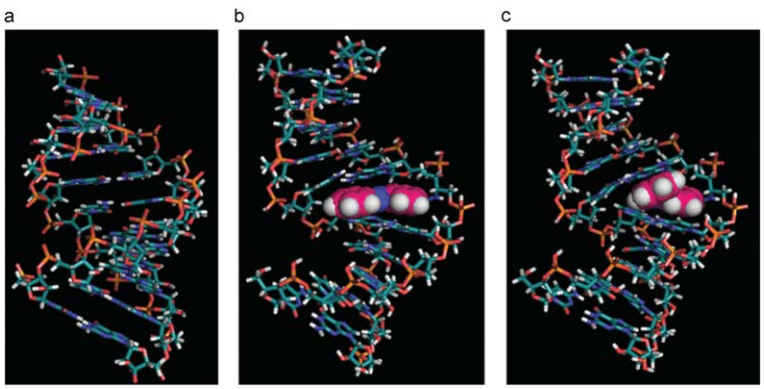

Fig. 4 Energy-minimized structure of native RNA/RNA duplex **R_nG/R_cC** (a), *trans*-**R_XG/R_cC** (b), and *cis*-**R_XG/R_cC** (c). The azobenzene moieties are shown as a space-filled model.

Table 3 Melting temperatures (T_m) of duplexes involving methyl-modified azobenzene

Duplex	T_m/°C[a]		
	trans	*cis*	ΔT_m
$\mathbf{R_XG/R_cC}$	48.8	36.5	12.3
$\mathbf{R_YG/R_cC}$	49.7	36.4	13.3
$\mathbf{R_ZG/R_cC}$	49.2	34.9	14.3
$\mathbf{D_XG/D_cC}$	42.9	35.6	7.3
$\mathbf{D_YG/D_cC}$	45.2	32.4	12.8
$\mathbf{D_ZG/D_cC}$	45.1	24.6	20.5

[a] Conditions: 5 μM dsRNA or dsDNA, 100 mM NaCl, 10 mM phosphate buffer (pH 7.0). The value of the measurement error was estimated within ± 0.3 °C.

a larger distortion occurred, especially for the two adjacent base pairs. A large steric hindrance with both base pairs and backbone may destabilize the duplex structure greatly. Again, the rigid A-form structure of the RNA/RNA duplex seems more sensitive to steric hindrance induced by *trans*-to-*cis* isomerization of azobenzene than the B-form structure of the DNA duplex.

Effect of methyl-modification of azobenzene on photoregulation of RNA hybridization

As reported previously, by introducing methyl groups into the *ortho* positions of azobenzene (Scheme 1), the photoregulatory efficiency of DNA hybridization is significantly improved, especially when methyl groups are introduced to both *ortho* positions on the distal benzene ring.[9] For RNA hybridization studied here, as compared with the unmodified azobenzene, the *trans*-form of modified azobenzene with methyl groups should stabilize the duplex more due to an increase of stacking interactions with the base pairs. On the other hand, remarkable destabilization can be expected in the *cis*-form because of the increase of steric hindrance. Another merit of 2′,6′-dimethylazobenzene is the high thermal stability of its *cis*-form, whose half-life is 10 times longer than that of non-modified azobenzene (**X**).[9] For example the half-life of *cis*-2′,6′-dimethylazobenzene involved in DNA is about 10 days at 37 °C.[9] Assuming that a similar effect can be expected in the case of photoregulation of RNA hybridization, 2′-methylazobenzene (**Y**) and 2′,6′-dimethylazobenzene (**Z**) were also introduced into RNA (see Scheme 1 for the structures). The results of T_m measurement showed that the ΔT_m of $\mathbf{R_YG/R_cC}$ and $\mathbf{R_ZG/R_cC}$ were 1.0 °C and 2.0 °C higher than that of $\mathbf{R_XG/R_cC}$, respectively (Table 3). Although the improvement of photoregulatory efficiency was not as large as that of photoresponsive DNA ($\mathbf{D_YG}$ and $\mathbf{D_ZG}$), the methyl modification was still favourable for photoregulation of RNA hybridization to some extent. The smaller effect can also be explained by the difficulty of intercalation of azobenzene into base pairs of the rigid A-form RNA/RNA duplex. When a long reaction time (>24 h) is necessary, 2′,6′-dimethylazobenzene-modified RNA is promising for clear-cut photoregulation of RNA functions, and the effect of thermal isomerisation can be disregarded.

Conclusions

We achieved efficient photoregulation of RNA hybridization by introducing azobenzene into RNA strands *via* D-threoninol, irrespective of the sequence. The photoregulatory efficiency of azobenzene-tethered RNA for RNA/RNA duplex formation is actually much better than that of photoresponsive DNA. Although *trans*-azobenzene destabilizes the RNA/RNA duplex to some extent due to the rigid A-form structure, the drastic destabilization effect of *cis*-azobenzene contributes to efficient photoregulation. By using this photoresponsive RNA, various RNA functions such as the regulation of gene expression with ribozymes, RNAi, and riboswitches can potentially be reversibly regulated with simple light irradiation. The efficient photoregulation can also be expected due to the structure change caused by *trans–cis* photoisomerization even in the case that RNA/RNA duplex is not completely dissociated in *cis*-form.[6a,19] Currently, photoregulation of gene expression in human cells by an RNAi approach is underway.

Experimental Section

Materials

Phosphoramidite monomers carrying azobenzene and its derivatives were synthesized as previously described.[7b] All conventional phosphoramidite monomers, CPG columns, the reagents for DNA and RNA synthesis, and Poly-Pak cartridges were purchased from Glen Research Co. Some native DNAs ($\mathbf{D_nG}$ and $\mathbf{D_cC}$) and RNAs ($\mathbf{R_cU}$, $\mathbf{R_cA}$, and $\mathbf{R_cG}$) were purchased from Integrated DNA Technologies, Inc.

Synthesis and purification of oligonucleotides

All azobenzene-tethered oligonucleotides were synthesized on an ABI 3400 DNA/RNA Synthesizer by using typical phosphoramidite chemistry as described in a previous report.[7b] Synthesized DNA was purified by Poly-Pak cartridges and reversed-phase HPLC (Merck LiChrospher 100 RP-18(e) column). For RNA synthesis, 2′-*O*-*t*-butyldimethylsilyl (TBDMS) protected RNA amidite monomers were used with a Trityl-off strategy. Removal of 2′-*O*-TBDMS was accomplished using tetra-*n*-butylammonium fluoride (TBAF) and then desalted by NAP Columns (GE Healthcare NAP-10 Columns). All RNAs were finally purified by 20% polyacrylamide-8M UREA gel electrophoresis followed by reverse-phase HPLC. After purification, synthesized oligonucleotides were characterized by MALDI-TOF MS.

Results of MALDI-TOF MS

m/z calcd for $\mathbf{R_nG}$ [*M*-H$^+$]: 3119; found: 3120; *m/z* calcd for $\mathbf{R_cC}$ [*M*-H$^+$]: 3182; found: 3184; *m/z* calcd for $\mathbf{R_XG}$ [*M*-H$^+$]: 3495; found: 3496; *m/z* calcd for $\mathbf{R_YG}$ [*M*-H$^+$]: 3391; found: 3393; *m/z* calcd for $\mathbf{R_ZG}$ [*M*-H$^+$]: 3523; found: 3524; *m/z* calcd for $\mathbf{R_XA}$ [*M*-H$^+$]: 3789; found: 3480; *m/z* calcd for $\mathbf{R_XU}$ [*M*-H$^+$]: 3456; found: 3456; *m/z* calcd for $\mathbf{R_XC}$ [*M*-H$^+$]: 3454; found: 3456; *m/z* calcd for $\mathbf{D_XG}$ [*M*-H$^+$]: 3377; found: 3378; *m/z* calcd for $\mathbf{D_YG}$ [*M*-H$^+$]: 3391; found: 3394; *m/z* calcd for $\mathbf{D_ZG}$ [*M*-H$^+$]: 3405; found: 3406.

Photoisomerization of azobenzene and its derivatives

The light source for photoirradiation was a 150 W Xenon lamp. For the *trans* → *cis* isomerization, a UV-D36C filter (Asahi Tech. Co.) was used, and UV light (λ = 300–400 nm; 5.3 mW cm^{-2} was used to irradiate the solution of the duplex at 60 °C for 3 min.

The *cis* → *trans* isomerization was carried out by irradiation with visible light ($\lambda > 400$ nm) through an L-42 filter (Asahi Tech. Co.) at 25 °C for 1 min. In both cases, a water filter was used to cut off the infrared light.

Spectroscopic measurement

UV–Vis spectra and circular dichroism (CD) spectra were measured with a JASCO model V-530 or V-550 UV–Vis and with a JASCO model V-820 CD spectrophotometer, respectively. Both instruments were equipped with programmed temperature controllers. Conditions of the sample solutions were as follows: [NaCl] = 100 mM, pH 7.0 (10 mM phosphate buffer), [DNA] = 5 μM.

Measurement of melting temperature

The melting curves of the duplexes were obtained by using the above UV–Vis apparatus to measure the change in absorbance at 260 nm *vs.* temperature, in which the temperature ramp was 1.0 °C min^{-1}. The T_m values were determined from the maximum in the first derivatives of the melting curves. Heating and cooling curves were measured, and the T_m values thus obtained coincided with each other within 2.0 °C. The T_m values presented here are an average of 2–4 independent experiments.

Determination of thermodynamic parameters

The enthalpy change ($\Delta H°$) and the entropy change ($\Delta S°$) for duplex formation were determined according to eqn (1).[14]

$$T_m^{-1} = (2.30R/\Delta H°) \log(C_t/4) + (\Delta S°/\Delta H°) \quad (1)$$

where C_t is the total concentration of both strands composing the duplex (R is the gas constant). The C_t values were varied from 1.0 to 32 μM. The change of Gibbs free energy at 37 °C ($\Delta G°$ (310 K)) was calculated from the $\Delta H°$ and the $\Delta S°$.

NMR measurements

NMR samples were prepared by dissolving three times lyophilized DNA, which contained both strands of a duplex, in a H_2O/D_2O 9/1 solution containing 10 mM sodium phosphate (pH 7.0), and the concentration of the duplex was adjusted to 1.0 mM. NaCl was added to a total sodium concentration of 200 mM. After NMR measurements in H_2O/D_2O, the samples were lyophilized again and dissolved in a D_2O solution. NMR spectra were measured by using a Varian INOVA spectrometer (700 MHz) equipped for triple resonance at a probe temperature of 280 K. 2D NOESY (mixing time of 150 ms) spectra[15] in H_2O/D_2O 9/1 were recorded by using the States-TPPI method[16] and a 3-9-19 WATERGATE pulse sequence for water suppression. FIDs (128 scans of each) of 2 K data points in the t_2 domain were collected for 512 data points in the t_1 domain. Prior to Fourier transformation, the spectra were zero-filled to give final 2 K × 1 K data points after apodization with a π/2-sifted squared sinebell function. 2D NOESY (mixing time of 100 and 200 ms), TOCSY (mixing time of 60 ms),[17] and DQF-COSY spectra[18] in D_2O were recorded by using the States-TPPI method without suppression of the H_2O signal. FIDs of the 2 K data points in the t_2 domain were collected for 512 data points in the t_1 domain. The number of scans for NOESY, TOCSY, and DQF-COSY in D_2O was 96. Prior to Fourier transformation, Gaussian window functions were applied to both dimensions.

Molecular modelling

The Insight II/Discover 98.0 program package was used for molecular modelling to obtain energy-minimized structures. The azobenzene residue was built by using the graphical program. The effects of water and counter ions were simulated by a sigmoidal, distance-dependant, dielectric function. The A-type duplex was used as the initial structure, and AMBER force fields were used for calculation. Computations were carried out on a Silicon Graphics O2 workstation with the operating system IRIX64 Release 6.5. As an initial calculation structure, an azobenzene moiety (either *trans* or *cis* form) was placed between the base pairs.

Acknowledgements

This work was supported by a Grant-in-Aid for Scientific Research from the Ministry of Education, Culture, Sports, Science and Technology, Japan. Partial support was also provided by Core Research for Evolution Science and Technology (CREST), Japan Science and Technology Agency (JST). Supporting Information is available online† or from the author.

References

1 (*a*) J. S. Mattick, *BioEssays*, 2003, **25**, 930; (*b*) J. S. Mattick and I. V. Makunin, *Hum. Mol. Genet.*, 2006, **15**, R17.
2 J. A. Doudna and T. R. Cech, *Nature*, 2002, **418**, 222.
3 D. P. Bartel, *Cell*, 2004, **116**, 281.
4 (*a*) A. Fire, S. Xu, M. K. Montgomery, S. A. Kostas, S. E. Driver and C. C. Mello, *Nature*, 1998, **391**, 806; (*b*) J. Kurreck, *Angew. Chem., Int. Ed.*, 2009, **48**, 1378.
5 C. A. Stein and Y. C. Cheng, *Science*, 1993, **261**, 1004.
6 (*a*) G. Mayer and A. Heckel, *Angew. Chem., Int. Ed.*, 2006, **45**, 4900; (*b*) J. P. Casey, R. A. Blidner and W. T. Monroe, *Mol. Pharm.*, 2009, **6**, 669.
7 (*a*) H. Asanuma, X. Liang, H. Nishioka, D. Matsunaga, M. Z. Liu and M. Komiyama, *Nat. Protoc.*, 2007, **2**, 203; (*b*) H. Kashida, X. G. Liang and H. Asanuma, *Curr. Org. Chem.*, 2009, **13**, 1065, and references cited therein.
8 X. G. Liang, H. Nishioka, N. Takenaka and H. Asanuma, *ChemBioChem*, 2008, **9**, 702.
9 (*a*) H. Nishioka, X. G. Liang, H. Kashida and H. Asanuma, *Chem. Commun.*, 2007, 4354; (*b*) H. Nishioka, X. G. Liang and H. Asanuma, *Chem.–Eur. J.*, 2010, **16**, 2054.
10 X. G. Liang, H. Asanuma, H. Kashida, A. Takasu, T. Sakamoto, G. Kawai and M. Komiyama, *J. Am. Chem. Soc.*, 2003, **125**, 16408.
11 (*a*) W. D. Wilson, L. Ratmeyer, M. Zhao, L. Strekowski and D. Boykin, *Biochemistry*, 1993, **32**, 4098; (*b*) M. Nakamura, Y. Fukunaga, K. Sara, Y. Ohtoshi, K. Kanaori, H. Hayashi, H. Nakano and K. Yamana, *Nucleic Acids Res.*, 2005, **33**, 5887.
12 J. SantaLucia, *Proc. Natl. Acad. Sci. U. S. A.*, 1998, **95**, 1460.
13 G. Reid Bishop and J. B. Chaires, *Current Protocols in Nucleic Acid Chemistry*, 2002, p. 7.11.1.
14 N. Sugimoto, Y. Shintani and M. Sasaki, *Chem. Lett.*, 1991, 1287.
15 J. Jeener, B. H. Meier, P. Bachmann and R. R. Ernst, *J. Chem. Phys.*, 1979, **71**, 4546.
16 D. Marion, M. Ikura, R. Tschudin and A. Bax, *J. Magn. Reson.*, 1989, **85**, 393.
17 C. Griesinger, G. Otting, K. Wuthrich and R. Freeman, *J. Am. Chem. Soc.*, 1988, **110**, 7870.
18 A. J. Shaka and R. Freeman, *J. Magn. Reson.*, 1983, **51**, 169.
19 (*a*) D. D. Young and A. Deiters, *Org. Biomol. Chem.*, 2007, **5**, 999; (*b*) X. J. Tang and I. J. Dmochowski, *Mol. BioSyst.*, 2007, **3**, 100; (*c*) M. Z. Liu, H. Asanuma and M. Komiyama, *J. Am. Chem. Soc.*, 2006, **128**, 1009; (*d*) X. G. Liang, R. Wakuda, K. Fujioka and H. Asanuma, *FEBS J.*, 2010, **277**, 1551.

